

Structural characterization of human cholesterol 7 α -hydroxylase

Wolfram Tempel,* Irina Grabovec,[†] Farrell MacKenzie,* Yaroslav V. Dichenko,[†] Sergey A. Usanov,[†] Andrei A. Gilep,[†] Hee-Won Park,[§] and Natallia Strushkevich^{1,†}

Structural Genomics Consortium,* University of Toronto, Toronto, Ontario, M5G 1L7, Canada; Institute of Bioorganic Chemistry NAS of Belarus,[†] Minsk, 220141 Belarus; and Department of Biochemistry and Molecular Biology,[§] Tulane University School of Medicine, New Orleans, LA 70112

Abstract Hepatic conversion to bile acids is a major elimination route for cholesterol in mammals. CYP7A1 catalyzes the first and rate-limiting step in classic bile acid biosynthesis, converting cholesterol to 7 α -hydroxycholesterol. To identify the structural determinants that govern the stereospecific hydroxylation of cholesterol, we solved the crystal structure of CYP7A1 in the ligand-free state. The structure-based mutation T104L in the B' helix, corresponding to the nonpolar residue of CYP7B1, was used to obtain crystals of complexes with cholest-4-en-3-one and with cholesterol oxidation product 7-ketocholesterol (7KCh). The structures reveal a motif of residues that promote cholest-4-en-3-one binding parallel to the heme, thus positioning the C7 atom for hydroxylation. Additional regions of the binding cavity (most distant from the access channel) are involved to accommodate the elongated conformation of the aliphatic side chain. Structural complex with 7KCh shows an active site rigidity and provides an explanation for its inhibitory effect. Based on our previously published data, we proposed a model of cholesterol abstraction from the membrane by CYP7A1 for metabolism. **■** CYP7A1 structural data provide a molecular basis for understanding of the diversity of 7 α -hydroxylases, on the one hand, and cholesterol-metabolizing enzymes adapted for their specific activity, on the other hand.—Tempel, W., I. Grabovec, F. MacKenzie, Y. V. Dichenko, S. A. Usanov, A. A. Gilep, H-W. Park, and N. Strushkevich. **Structural characterization of**

human cholesterol 7 α -hydroxylase. *J. Lipid Res.* 2014. 55: 1925–1932.

Supplementary key words cytochrome P450 • X-ray crystallography CYP7A1 • oxysterols

The formation of bile salts in the liver is the quantitatively most important pathway of cholesterol elimination from the body (1, 2). Other pathways of cholesterol metabolism include the conversion of cholesterol into steroid hormones and vitamin D₃. The maintenance of cholesterol homeostasis in various tissues and cells requires complex interactions of a number of physiological factors (3, 4), including several cholesterol-metabolizing enzymes of the cytochrome P450 family (CYP).

Cytochrome P450 proteins utilize heme cofactor to perform oxidation chemistry with a vast diversity of drugs and endogenous molecules, including steroids, vitamin D, and eicosanoids. Membrane-bound CYPs localized either in the endoplasmic reticulum or mitochondria, where they use different redox partners to shuttle electrons from NADPH to molecular oxygen, resulting in the insertion of one atom of oxygen into the substrate while the other oxygen atom is reduced to water (5). The active site is buried in the core of the protein and presents a preformed cavity above the heme connected to the surface through a channel. Despite a unique but rather conserved P450-fold, the molecular mechanisms of CYP substrate specificity and selectivity remain elusive.

Cholesterol oxidation products, especially 7-ketocholesterol (7KCh), are highly toxic and associated with chronic diseases including atherosclerotic and neurodegenerative processes (6, 7). 7KCh has potent pharmacological properties to induce inflammation and apoptosis (8). As a photooxidation product of nonenzymatic and possibly enzymatic

The SGC is a registered charity (number 1097737) that receives funds from AbbVie, Bayer, Boehringer Ingelheim, the Canada Foundation for Innovation, the Canadian Institutes for Health Research, Genome Canada through the Ontario Genomics Institute [OGI-055], GlaxoSmithKline, Janssen, Lilly Canada, the Novartis Research Foundation, the Ontario Ministry of Economic Development and Innovation, Pfizer, Takeda, and the Wellcome Trust [092809/Z/10/Z]. Diffraction data for the substrate-free crystal were measured at beamline X25 of the National Synchrotron Light Source, which is principally by the Offices of Biological and Environmental Research and of Basic Energy Sciences of the US Department of Energy, and the National Center for Research Resources (P41RR012408) and the National Institute of General Medical Sciences (P41GM103473) of the National Institutes of Health. Institutes Structural Biology Facility at the Advanced Photon Source (GM/CA @ APS) has been funded in whole or in part with federal funds from the National Cancer Institute (Y1-CO-1020) and the National Institute of General Medical Sciences (Y1-GM-1104). Use of the Advanced Photon Source was supported by the US Department of Energy, Basic Energy Sciences, Office of Science, under Contract No. DE-AC02-06CH11357.

Manuscript received 7 May 2014 and in revised form 7 June 2014.

Published, JLR Papers in Press, June 13, 2014
DOI 10.1194/jlr.M050765

Copyright © 2014 by the American Society for Biochemistry and Molecular Biology, Inc.

This article is available online at <http://www.jlr.org>

Abbreviations: 7KCh, 7-ketocholesterol; CYP, cytochrome P450; RMSD, root mean square deviation.

¹To whom correspondence should be addressed.
e-mail: natstrush@gmail.com

pathways in the retina, 7KCh might be a pathogenetic factor in age-related macular degeneration (9). The major routes for 7KCh metabolism include *a*) conversion into less toxic 27-hydroxylated 7KCh by CYP27A1/CYP46A1 (10–13) and further to more water-soluble metabolites, thus protecting mitochondria from reactive oxygen species; *b*) esterification including sulfonation (14); *c*) lipoprotein-mediated elimination (15); and *d*) interconversion to 7 β -hydroxycholesterol by 11 β -hydroxysteroid dehydrogenase type 1 (16, 17). However, the mechanisms of 7KCh formation and elimination are still not fully understood.

Conversion of cholesterol into 7 α -hydroxycholesterol by CYP7A1 represents the first and rate-limiting step in the classic pathway of bile salts biosynthesis. Hydroxylation of the ring system of cholesterol in a regio- and stereospecific manner with further oxidation and shortening of the side chain produces water-soluble bile acids with powerful detergent properties to emulsify dietary lipids (4). Bile acids also serve as signaling molecules that bind to G-protein-coupled receptors (GPCRs) and nuclear hormone receptors that regulate lipid, glucose, and energy metabolism (18). A modulation of both oxysterol and bile acid signaling pathways has recently emerged as a source of promising novel drug targets to treat common metabolic and hepatic diseases (19).

Bile acid synthesis is tightly regulated through the transcriptional regulation of CYP7A1 (1) and possibly by the availability of substrate to the enzyme, which is located in the cholesterol-poor endoplasmic reticulum (20). In humans, three cytochrome P450 enzymes perform the 7 α -hydroxylation reaction: CYP7A1 is specific for cholesterol, CYP7B1 for oxysterols and steroids, and CYP39A1 for 24(S)-hydroxycholesterol. None of these 7 α -hydroxylases are structurally characterized, hindering understanding of the molecular mechanisms of their substrate selectivity. Here we present crystal structures of CYP7A1, both unliganded and bound to either the substrate cholest-4-en-3-one or the inhibitor 7KCh. Ligands are bound deep in the active site cavity, isolated from the bulk solvent, in a previously unobserved orientation complemented by unusual structural features of CYP7A1. An asparagine (Asn) residue in place of the highly conserved threonine (Thr) in I helix does not directly interact with cholest-4-en-3-one. Instead, the Asn residue appears to interact with the sixth ligand of the heme iron in the ligand-free and 7KCh structures. Maintaining the network involving the 7-keto group and interaction with the protein's active site residues along with closed conformation of the access channel explain a competitive inhibition by 7KCh. Combining these new findings with previous data prompted us to suggest a working model for cholesterol binding by CYP7A1 from the membrane.

MATERIALS AND METHODS

CYP7A1 protein expression and purification

The CYP7A1 cDNA was purchased from Origene [accession code TC123882 (NM_000780)] and subcloned into a modified pCW-LIC vector. The N-terminal transmembrane anchor domain

(codons 1–24) was replaced with an optimized sequence, MAKKTSS. The C-terminally His₅-tagged protein was coexpressed with GroEL/ES (pGro12, Takara Bio Inc.) in *Escherichia coli* JM109. Cells were lysed by passing through a Microfluidizer (Microfluidics Corp.) at 18,000 psi. Sodium cholate was added to the lysate at a final concentration of 23 mM, and the lysate was incubated at 4°C for 1 h. After centrifugation at 60,000 *g* for 1 h, protein was purified using metal affinity chromatography on a HiTrap chelating column charged with Ni²⁺ (Amersham Biosciences) and cation-exchange chromatography using a Source 30S column (Amersham Biosciences). The protein storage buffer was 50 mM potassium phosphate buffer, pH 7.4, 20% glycerol, and 0.5 M NaCl. The molecular mass of purified protein measured by ESI-MS was 56,255 Da (expected 56,257 Da). The spectrophotometric index OD 418/OD280 of purified sample used in crystallization trials was 1.5. A total P450 protein concentration was determined from reduced CO difference spectra (21).

Protein crystallization

Purified CYP7A1 was crystallized in the presence of 100 μ M cholesterol using the hanging drop vapor diffusion method at 18°C after mixing 1 μ l of the protein solution with 1 μ l of the reservoir solution containing 0.1 M sodium chloride, 0.1 M trisodium citrate pH 5.5, and 20% polyethylene glycol (PEG) 400. Crystals were soaked with 30% glycerol as cryoprotectant before flash freezing in liquid nitrogen. To obtain a complex with cholest-4-en-3-one, a T104L mutant was used, and the crystals were grown in conditions containing 0.1 M MES pH 6.0 and 18% PEG 550 monomethylether (MME) at room temperature and soaked with 20% glycerol for flash freezing in liquid nitrogen. For the T104L mutant-7KCh complex, crystals were grown in 0.1 M sodium chloride, 0.1 M tri-sodium citrate pH 5.6, and 20% PEG 400.

Structure determination and refinement

Crystallographic methods and results are summarized in **Table 1**. Diffraction data were collected at 100 K at synchrotron radiation sources. The ligand-free structure was solved by molecular replacement with PHASER (22) and a search model derived from Protein Data Bank (PDB) entry 2IAG (23). Density-modified maps from RESOLVE (24) guided pruning of the initial model. Molecular replacement with an intermediate model and MOLREP (25) produced the current orientation of the model in the unit cell. The ligand-free structure subsequently served as search model for molecular replacement solution of the complex structures with PHASER. Restraints for substrate geometry were calculated with PRODRG (26).

Spectral binding assay

Ligand binding affinities were determined with the spectral-ligand binding assay as described previously (27).

Enzyme assays

The 7 α -hydroxylase activity of CYP7A1. Activity was measured in the reconstituted system at 37°C in 25 mM Hepes buffer pH 7.2 containing 0.1 mM DTT, 0.1 mM EDTA, 4 mM MgCl₂, and 0.15% sodium cholate. The aliquots of concentrated recombinant proteins were mixed and preincubated for 5 min at room temperature. The final concentrations of CYP7A1 and NADPH-cytochrome P450 reductase (CPR) were 0.5 and 1.0 μ M, respectively. Cholest-4-en-3-one (10 mM in 45% hydroxypropyl-beta-cyclodextrin, HPCD) was added to the reaction mixture at a final concentration of 50 μ M. After 10 min of preincubation at 37°C, the reaction was started by adding NADPH to a final concentration of 0.25 mM. Aliquots (0.5 ml) were taken from the incubation mixture at selected time intervals. Steroids were extracted with 5 ml

TABLE 1. Data collection and refinement statistics

Ligand	None	Cholest-4-en-3-one	7KCh
PDB code	3DAX	3SN5	3V8D
X-ray source	NLSL-X25	APS 23IDB	CLS 08ID (46)
Wavelength [Å]	0.9686	0.9793	0.9762
Cell a, b, c [Å]	55.34, 80.16, 84.94	56.16, 137.63, 160.15	55.62, 74.22, 87.93
Cell α , β , γ [°]	64.36, 75.23, 72.17	90.00, 90.00, 90.00	66.33, 75.53, 69.62
Space group	P1	P2 ₁ 2 ₁	P1
Data reduction software	DENZO, SCALEPACK (47) ^a	XDS, XSCALE (48)	DENZO, SCALEPACK ^a
Resolution limits (outer shell) [Å]	38.01–2.11 (2.16–2.11)	30.00–2.75 (2.82–2.75)	43.67–1.90 (1.93–1.90)
Completeness [%]	91.7 (63.0)	99.8 (100.0)	97.2 (89.0)
Redundancy	3.7 (3.1)	7.4 (7.5)	3.8 (3.7)
Rmerge	0.063 (0.427)	0.098 (0.990)	0.075 (1.042)
<I/ σ (I)>	13.1 (2.5)	14.2 (2.4)	10.7 (1.2)
Molecular replacement model	PDB:2IAG	PDB:3DAX	PDB:3DAX
Final refinement software	REFMAC (49)	AUTOBUSTER (50) (51)	REFMAC
Refinement resolution [Å]	30.00–2.15	29.58–2.75	43.67–1.90
Number of reflections in work/free set	61,020/2,018	31,339/1,775	90,113/2,066
Rwork/Rfree	0.189/0.228	0.182/0.220	0.185/0.225
Number of refined atoms/average B-factor [Å ²] ^b	7,737/38.0	7,357/77.6	8,115/31.2
Protein	7,519/38.3	7,215/78.0	7,584/31.1
Heme	86/29.4	86/52.5	86/22.3
Substrate	None	56/56.2	58/21.6
RMSD bonds [Å]/angles [°]	0.017/1.3	0.009/1.0	0.014/1.4
Molprobt favored/outliers [%] ^c	98.6/0.0	97.6/0.1	98.7/0.1

RMSD, root mean square deviation.

^aScaled reflection statistics calculated using POINTLESS/AIMLESS (52).

^bPHENIX.PDBTOOLS (53).

^cPHENIX.RAMALYZE (53).

of methylene chloride. After vigorous mixing, aqueous and organic layers were separated by centrifugation at 3,000 rpm for 10 min. The organic layer was carefully removed and dried under argon flow. Methanol (100 μ l) was added to the resulting pellet, and steroids were analyzed on an HP1090 liquid chromatograph equipped with a Bondapak C18-column (3.9 \times 300 mm) or an LC-MS system (Thermo Accela HPLC system with LCQ-Fleet MS system). The 7 α -hydroxylase activity in the presence of 7KCh was measured in the reconstituted system, which includes 0–100 μ M of 7KCh as described previously.

RESULTS AND DISCUSSION

Overall structure of CYP7A1

CYP7A1 exhibited a typical cytochrome P450-fold with the conserved structural core of helices D, E, I, and L around the heme prosthetic group (**Fig. 1**). The most similar structures available in the PDB, identified using the DALI server, were prostacyclin synthase, CYP8A1 (PDB code 3B6H, 34% identity, 2.0 Å rmsd), and lanosterol 14-demethylase, CYP51 (PDB code 3JUS, 22% identity, 3.5 Å rmsd). Notably, CYP8A1 is a self-sufficient P450 (i.e., requires neither molecular oxygen nor NADPH reductase to perform its distinct isomerase reaction, as opposed to the typical monooxygenase reaction). However, another member of the CYP8 family, CYP8B1, as well as CYP7A1 and CYP7B1, is involved in bile acid biosynthesis and requires a cytochrome P450 reductase as an electron donor. Despite the divergent chemistry of their respective catalyzed reactions and different substrates, CYP7A1 shared common structural features with CYP8A1 (23). Specifically, the B' helix was approximately perpendicular to the

heme plane; a profound I helix kink disrupted the G helix at C term to form a separate G' helix; an Asn residue instead of the conserved Thr, which is involved in oxygen activation in most P450s; and a long meander region on the proximal surface, a site for the interaction with the redox partner (**Fig. 1A, B**). CYP7A1 was structurally less similar to CYP51, the evolutionary oldest P450, with the preserved function of sterol 14 α -demethylation in the cholesterol biosynthetic pathway.

Ligand-free CYP7A1 crystallized in the presence of cholesterol adopted a closed conformation with no obvious access channels. It is unclear whether the rigid and closed active site was a crystallization artifact or reflected the *in vivo* state of the enzyme in the absence of the substrate and/or certain physiological stimuli. Electron density maps showed some peaks in the putative substrate binding site, but density was too weak to enable placement of the substrate in the model. Additional efforts to cocrystallize and analyze WT CYP7A1 with a substrate failed to produce interpretable electron density for the cholesterol molecule.

An analysis of the closed conformation shows the location and orientation of residues lining the active site cavity and those residues that are likely to interact with the substrate. Structure-based sequence comparison of 7 α -hydroxylases reveals two polar residues, Thr104 and Ser105 of B' helix, as potential substrate recognition residues. The B' helix is known to control substrate specificity and generally displays considerable deviation in sequence and structural organization within the P450 family (28). The active site was not as nonpolar as expected for the binding of the hydrophobic cholesterol substrate. Therefore, we hypothesized that mutation of these active site polar residues to the corresponding nonpolar residues of CYP7B1

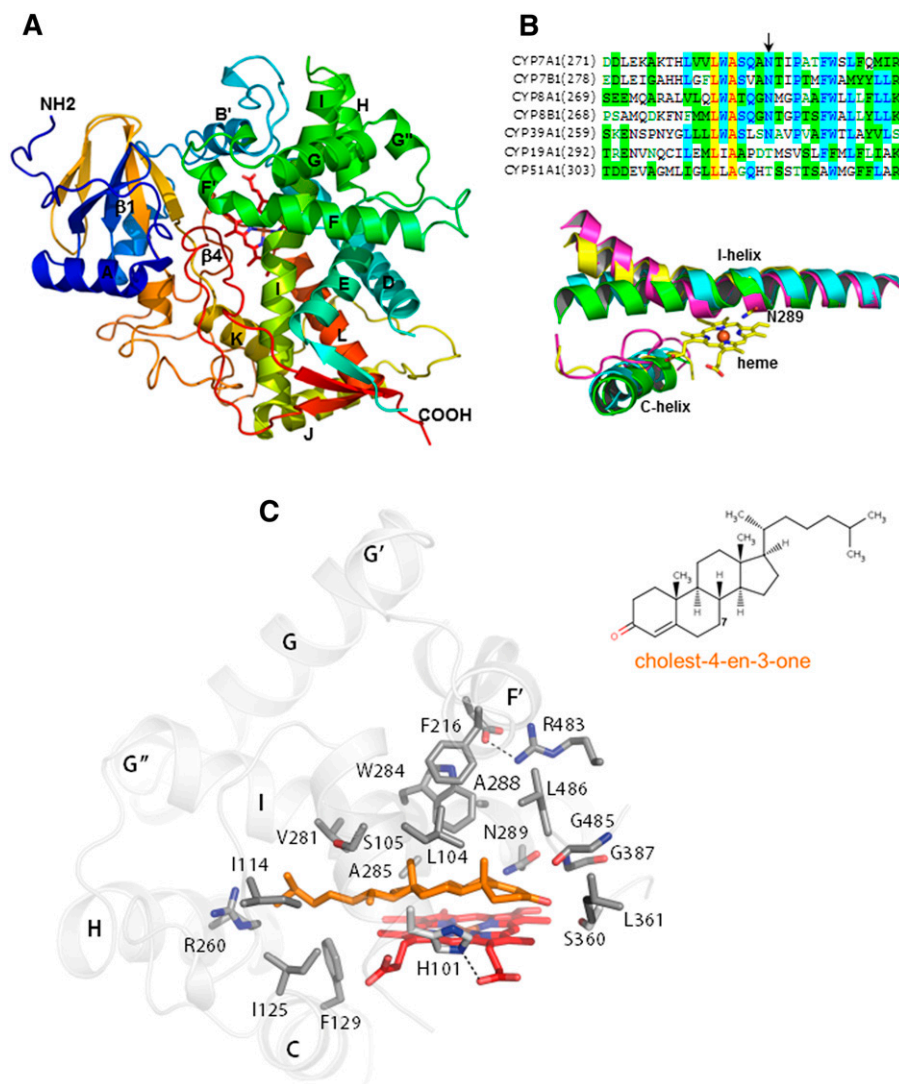


Fig. 1. CYP7A1 structure. A: Overall structure of CYP7A1 rainbow-colored from blue N terminus to the red C terminus. B: A sequence alignment and superposition of I helix in CYP7A1 (yellow), CYP19A1 (green, PDB code 3EQM), human CYP51A1 (blue, PDB code 3LD6), *Mycobacterium tuberculosis* CYP51 (pink, PDB code 1EA1) highlighting active site residue Asn289. C: CYP7A1 bound to cholest-4-en-3-one. Cholest-4-en-3-one (orange) is surrounded by 16 residues within 4 Å from different structural elements: B' helix (H101, T104L, S105), B-C loop (I114), C helix (I125 and F129), H helix (R260), I helix (V281, W284, A285, and N289), the loop between the K helix and β 1–4 strand (S360 and L361), and the loop between two β 4 strands at the C terminus (G485, L486, and G487).

could be favorable for interaction with cholesterol and thus render the protein more amenable to cocrystallization. We designed and analyzed mutant protein T104L and solved crystal structures of its complexes with cholest-4-en-3-one and 7KCh.

Substrate recognition

CYP7A1 can bind and hydroxylate cholesterol and cholest-4-en-3-one with high efficiency as well as oxysterols (**Table 2**) (29). The T104L mutant was similar to WT in binding and catalytic properties (**Table 2**) and readily crystallized with substrates. The structure of the T104L mutant in complex with cholest-4-en-3-one explicitly identified key residues involved in 7α -hydroxylation. Cholest-4-en-3-one bound parallel to the heme with the α -side of the steroid

nucleus facing the heme plane at a distance of ~ 3.5 Å (Fig. 1C). The substrate was positioned above the heme propionates rather than the pyrrole rings. This “pushing” of the substrate toward the B' helix is caused by W284 and N289 of I helix that protrude into the active site. As a result, the aliphatic chain of cholest-4-en-3-one was bound in the hydrophobic pocket formed by H helix, bent I helix, and the extended B-C loop; whereas the C7 carbon of the steroid B-ring was 5 Å away from the heme iron for stereospecific oxidation.

The hydrophobic side chain of the T104L mutant in the B' helix provided additional favorable van der Waals contact with the C19 methyl group of cholest-4-en-3-one. Notably, T104L was located in the hydrophobic environment of V220 and L486, residues known to affect substrate binding

TABLE 2. Binding and activity of WT and T104L mutant

Form	Cholesterol		4-Cholesten-3-one		25OH-CH		27OH-CH	
	K_b , μM	Turnover, min^{-1}	K_b , μM	Turnover, min^{-1}	K_b , μM	Turnover, min^{-1}	K_b , μM	Turnover, min^{-1}
WT	1.85 ± 0.18	0.48 ± 0.02	0.14 ± 0.03	0.17 ± 0.04	NS	0.89 ± 0.15	NS	4.11 ± 0.15
T104L	1.04 ± 0.07	1.38 ± 0.12	0.08 ± 0.009	0.36 ± 0.10	NS	—	NS	7.03 ± 0.27

NS, no or weak spectral response. The spectral response, $A_{390-420}$, was <0.005 absorbance units when $1 \mu\text{M}$ P450 was titrated with up to a $50 \mu\text{M}$ steroid.

and metabolism (30, 31), thus stabilizing the T104L mutation.

As noted previously, the active site volume and positioning of the substrate was controlled by bulky W284, positioned above the C6-C7 bond of cholest-4-en-3-one. The indole moiety of W284 was sandwiched between F216 (F' helix) and A288 (I helix) and interacted with D213 (F helix), which also formed a salt bridge with R483 near the protein surface. This interaction network seems to be important for the proper function, as evident from the R486C mutation of homologous CYP7B1, which is linked to neurodegenerative disease (32). In CYP7A1, the mutation W284F but not W284Y has been shown to abolish a spectral response to cholesterol (31), indicating the requirement of this residue to maintain the local network for proper positioning of the steroid ring scaffold near the heme. Residue W284 is conserved among microsomal sterol 7α -hydroxylases (CYP7B1, CYP8B1, and CYP39A1), as well as in CYP8A1, but is absent in P450s that catalyze cholesterol side chain hydroxylation (CYP11A1, CYP27A1, and CYP46A1). This finding is consistent with the role of the active site tryptophan as a “low ceiling” keeper (33), which is required for both monooxygenase (CYP7B1, CYP8B1, and CYP39A1) and isomerase (CYP8A1) activities.

Due to steric hindrance by W284, a steroid substrate cannot move any closer to the heme iron. Substitution of a “canonical” Thr for Asn in I helix may enable C7 regioselectivity of CYP7A1. From the multiple sequence alignment of >180 CYP7 proteins, we can deduce a new motif of LWAx xx NT in place of (A/G)GxxT, which is present in most P450s, and a different proton transfer pathway/mechanism is anticipated. A stable CO complex and the lack of heme movement upon substrate binding are typical features of P450s including CYP7A1, but not of CYP8A1 with P450-fold but non-P450 chemistry (34), which exhibits the highest structural homology with CYP7A1. The atypical Asn of CYP7A1 may have a slightly different function from that of CYP8A1. In CYP7A1, N289 was positioned within 3.8 \AA of C6 of cholest-4-en-3-one and may assist O-O bond cleavage in later steps of the catalytic cycle. On the other hand, the corresponding Asn of CYP8A1 stabilizes stereospecific substrate binding by a hydrogen bond with one of two chemically equivalent endoperoxide oxygen atoms, based on analysis of an analog. Moreover, binding of the substrate to the heme iron in CYP8A1 is accompanied by heme movement (34).

Cholest-4-en-3-one adopted an elongated conformation, and its keto oxygen was located $\sim 3.4 \text{ \AA}$ away from the amide link between S360 and L361. In the 7KCh complex structure, the 3β -hydroxyl hydrogen bonded with glycine

485, and this interaction would likely be preserved in cholesterol binding. This finding suggests that the presence of a hydroxyl or keto group at the C3 position is a significant determinant for substrate binding, consistent with previous studies (31).

Binding of cholest-4-en-3-one was accompanied by structural changes at the entrance of the access channel, mostly at the N terminus of the protein, where transition from a loop to A' helix conformation and the movement of the loop between $\beta 1$ and $\beta 2$ strands result in channel opening (Fig. 2A).

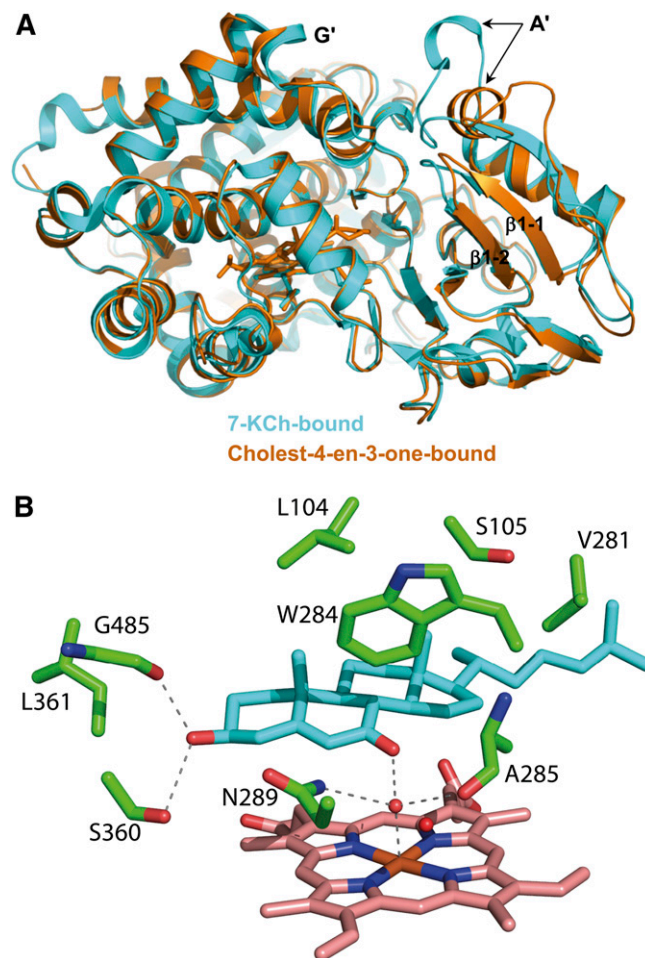


Fig. 2. A: Superposition of 7KCh-bound (cyan) with cholest-4-en-3-one-bound (brown) structure. Labeled regions show displacement and different conformation (A' helix). B: 7KCh binding. Selected residues, heme (salmon), and hydrogen bonding of 3β -OH and 7-keto groups of 7KCh (blue) are shown.

Structure in complex with 7KCh, a CYP7A1-specific inhibitor

7KCh is a strong competitive inhibitor of CYP7A1 ($IC_{50} \sim 1 \mu\text{M}$) (35) and recently has been reported to be the product of the CYP7A1 action on 7-dehydrocholesterol in vitro and possibly in vivo (36, 37). Inhibition of CYP7A1 activity, estimated in our standard reconstituted enzymatic reaction, was similar for WT CYP7A1 and the T104L mutant with $K_i(\text{app})$ at 5.6 μM and 6.8 μM , respectively.

To investigate the structural basis of CYP7A1 inhibition by 7KCh, we determined the crystal structure of the complex. Crystals were obtained with the T104L mutant under conditions similar to that for the ligand-free protein (see Materials and Methods). When compared with the ligand-free structure, the presence of 7KCh did not affect the overall conformation (rmsd 0.4 Å). The 7KCh-bound structure represents a closed conformation different from the semiopen cholest-4-en-3-one-bound structure (Fig. 2A). These ligand-specific structural differences suggest that conformational dynamics play an important role in substrate recognition. A possibility of resistance to conformational changes by the crystal packing in the 7KCh-bound structure, however, is not excluded.

The structure of the active site with 7KCh was virtually the same when compared with the substrate. The same set of residues packed against the steroid core and the side chain of 7KCh. In addition, the 3 β -OH group of 7KCh formed hydrogen bonds with G485 and the hydroxyl group of S360 (Fig. 2B). A water molecule is coordinating the heme iron, consistent with the result of the ligand binding assay, which showed no transition from low spin of the Soret band. Notably, the iron-coordinating water formed a hydrogen bond to the 7-keto group of the inhibitor and also to the Ala285 backbone carbonyl and the side chain of Asn289. This network might resemble the state during proton delivery to the heme-bound dioxygen with Asn289 serving as the key proton donor, although unproductive in the presence of the 7-keto group. Overall, the structural data are consistent with 7KCh competitive inhibition in functional assays and demonstrate that the same hydrophobic and polar interactions are utilized as for the substrate.

Structural adaptations for cholesterol hydroxylation by CYP7A1

Both ligand-bound CYP7A1 structures suggest that the steroid entered the active site with the side chain first. This binding orientation might be the evolutionary adaptation to access a cholesterol molecule from the membrane. We hypothesize that CYP7A1 is embedded into the outer leaflet of the membrane at a depth of approximately half of the lipid bilayer ($\sim 10\text{--}15 \text{ \AA}$). In this mode, the N-terminal transmembrane helix, the F-G loop, and the A' helix (membrane binding regions) face the cholesterol molecule from the inner leaflet of the membrane with cholesterol side chain oriented toward the entry point of the access channel (Fig. 3). Either certain stimuli (e.g., changing in local lipid composition) or interactions with other proteins may induce the conformational changes that

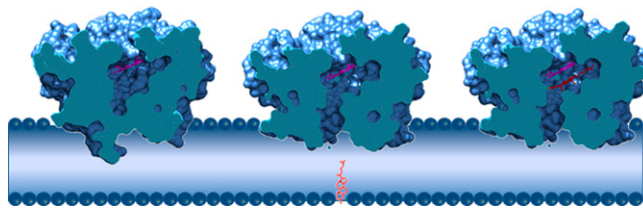



Fig. 3. A model of cholesterol abstraction from the membrane by CYP7A1 (surface representation). Several cross-sections of the active site and access channel are shown.

cause opening of the substrate access channel, into which cholesterol enters with its side chain leading. Further positioning in the active site would ensure that the position of cholesterol hydroxylation approaches the heme iron. Consistent with a generally accepted model for cholesterol substrate delivery directly from the membrane, this relatively straightforward binding model is supported by mutagenesis, chemical modification studies (28, 30, 38), and membrane penetration depth calculations (39–41). Interestingly, all available mammalian P450s structures of enzymes that hydroxylate sterol substrates (CYP11A1: PDB code 3N9Y, CYP46A1: PDB code 2Q9F, and CYP7A1: PDB code 3SN5), independent of the cholesterol hydroxylation position on the aliphatic chain or the ring system, show a conserved cholesterol orientation (side chain near the heme). The possibility of a cholesterol flip-flop from the membrane into the channel similar to cholesterol diffusion within the membrane (42, 43) cannot be excluded and warrants further investigation.

A unique feature of CYP7A1, compared with other cholesterol-metabolizing P450s, is a long meander region on the proximal side. This region acts as the electron transfer interface and contains the positively charged residues that appear to contribute to reductase binding. The meander is located close to the Cys-binding loop, which can modulate electronic properties of the heme and ultimately the catalytic function of CYP7A1 (44). An alternative positioning of the meander is observed in full-length yeast CYP51 in complex with lanosterol (45) and suggests the following: *a*) a significant flexibility of this region that enables its relocation for capping the Cys-binding loop and contacts with the C helix, thereby dramatically changing the electron transfer interface; and *b*) that it may interact with other protein effectors, which stimulate/regulate substrate binding. Modulation of the interaction interface by the longer meander might also be a feature of CYP7/8 proteins evolutionary closest to CYP51 and might be further adapted for nonmonooxygenase chemistry (e.g., self-sufficient CYP8A1).

In conclusion, CYP7A1 structures identify residues involved in cholest-4-en-3-one binding and specific interactions with the inhibitor 7KCh. Some structural features that have evolved to hydroxylate the cholesterol ring system are not unique to CYP7A1 and enable different chemistry in other CYPs. Following the general concept for cholesterol-metabolizing cytochrome P450s to acquire a substrate molecule from the membrane, we suggest that orientation of cholesterol in the different leaflets of the

lipid bilayer can be recognized for further binding by CYP7A1 alone or in complex with protein partners.

The coordinates and structure factors of the CYP7A1 structures have been deposited in the Research Collaboratory for Structural Bioinformatics PDB under the accession codes 3DAX, 3SN5 (in complex with cholest-4-en-3-one), and 3V8D (in complex with 7KCh) 

The authors thank Dr. Amy K. Wernimont for reviewing the model of the cholest-4-en-3-one complex structure, and T. Cherkasova for technical assistance.

REFERENCES

1. Chiang, J. Y. 1998. Regulation of bile acid synthesis. *Front. Biosci.* **3**: d176–d193.
2. Vlahcevic, Z. R., W. M. Pandak, and R. T. Stravitz. 1999. Regulation of bile acid biosynthesis. *Gastroenterol. Clin. North Am.* **28**: 1–25.
3. Chiang, J. Y. 2009. Bile acids: regulation of synthesis. *J. Lipid Res.* **50**: 1955–1966.
4. Russell, D. W. 2009. Fifty years of advances in bile acid synthesis and metabolism. *J. Lipid Res.* **50** (Suppl.): S120–S125.
5. Poulos, T. L., and E. F. Johnson. 2005. Structures of cytochrome P450 enzymes. In *Cytochrome P450: Structure, Mechanism and Biochemistry*. P. R. Ortiz de Montellano, editor. Kluwer Academic/Plenum Publishers, New York. 87–114.
6. Lyons, M. A., and A. J. Brown. 1999. 7-Ketocholesterol. *Int. J. Biochem. Cell Biol.* **31**: 369–375.
7. Brown, A. J., and W. Jessup. 1999. Oxysterols and atherosclerosis. *Atherosclerosis*. **142**: 1–28.
8. Vejux, A., and G. Lizard. 2009. Cytotoxic effects of oxysterols associated with human diseases: induction of cell death (apoptosis and/or oncosis), oxidative and inflammatory activities, and phospholipidosis. *Mol. Aspects Med.* **30**: 153–170.
9. Rodríguez, I. R., and I. M. Larrayoz. 2010. Cholesterol oxidation in the retina: implications of 7KCh formation in chronic inflammation and age-related macular degeneration. *J. Lipid Res.* **51**: 2847–2862.
10. Brown, A. J., G. F. Watts, J. R. Burnett, R. T. Dean, and W. Jessup. 2000. Sterol 27-hydroxylase acts on 7-ketocholesterol in human atherosclerotic lesions and macrophages in culture. *J. Biol. Chem.* **275**: 27627–27633.
11. Jessup, W., and A. J. Brown. 2005. Novel routes for metabolism of 7-ketocholesterol. *Rejuvenation Res.* **8**: 9–12.
12. Heo, G. Y., I. Bederman, N. Mast, W. L. Liao, I. V. Turko, and I. A. Pikuleva. 2011. Conversion of 7-ketocholesterol to oxysterol metabolites by recombinant CYP27A1 and retinal pigment epithelial cells. *J. Lipid Res.* **52**: 1117–1127.
13. Lyons, M. A., and A. J. Brown. 2001. Metabolism of an oxysterol, 7-ketocholesterol, by sterol 27-hydroxylase in HepG2 cells. *Lipids*. **36**: 701–711.
14. Fuda, H., N. B. Javitt, K. Mitamura, S. Ikegawa, and C. A. Strott. 2007. Oxysterols are substrates for cholesterol sulfotransferase. *J. Lipid Res.* **48**: 1343–1352.
15. Brown, A. J., and W. Jessup. 2009. Oxysterols: sources, cellular storage and metabolism, and new insights into their roles in cholesterol homeostasis. *Mol. Aspects Med.* **30**: 111–122.
16. Schweizer, R. A., M. Zurcher, Z. Balazs, B. Dick, and A. Odermatt. 2004. Rapid hepatic metabolism of 7-ketocholesterol by 11beta-hydroxysteroid dehydrogenase type I: species-specific differences between the rat, human, and hamster enzyme. *J. Biol. Chem.* **279**: 18415–18424.
17. Larsson, H., Y. Bottiger, L. Iuliano, and U. Diczfalussy. 2007. In vivo interconversion of 7beta-hydroxycholesterol and 7-ketocholesterol, potential surrogate markers for oxidative stress. *Free Radic. Biol. Med.* **43**: 695–701.
18. Chiang, J. Y. 2013. Bile acid metabolism and signaling. *Compr. Physiol.* **3**: 1191–1212.
19. Thomas, C., R. Pellicciari, M. Pruzanski, J. Auwerx, and K. Schoonjans. 2008. Targeting bile-acid signalling for metabolic diseases. *Nat. Rev. Drug Discov.* **7**: 678–693.
20. Straka, M. S., L. H. Junker, L. Zacarro, D. L. Zogg, S. Dueland, G. T. Everson, and R. A. Davis. 1990. Substrate stimulation of 7 alpha-hydroxylase, an enzyme located in the cholesterol-poor endoplasmic reticulum. *J. Biol. Chem.* **265**: 7145–7149.
21. Omura, T., and R. Sato. 1964. The carbon monoxide-binding pigment of liver microsomes. I. Evidence for its hemoprotein nature. *J. Biol. Chem.* **239**: 2370–2378.
22. McCoy, A. J., R. W. Grosse-Kunstleve, P. D. Adams, M. D. Winn, L. C. Storoni, and R. J. Read. 2007. Phaser crystallographic software. *J. Appl. Crystallogr.* **40**: 658–674.
23. Chiang, C. W., H. C. Yeh, L. H. Wang, and N. L. Chan. 2006. Crystal structure of the human prostacyclin synthase. *J. Mol. Biol.* **364**: 266–274.
24. Terwilliger, T. C. 2003. SOLVE and RESOLVE: automated structure solution and density modification. *Methods Enzymol.* **374**: 22–37.
25. Vagin, A., and A. Teplyakov. 2010. Molecular replacement with MOLREP. *Acta Crystallogr. D Biol. Crystallogr.* **66**: 22–25.
26. Schüttelkopf, A. W., and D. M. van Aalten. 2004. PRODRG: a tool for high-throughput crystallography of protein-ligand complexes. *Acta Crystallogr. D Biol. Crystallogr.* **60**: 1355–1363.
27. Strushkevich, N., F. MacKenzie, T. Cherkasova, I. Grabovec, S. Usanov, and H. W. Park. 2011. Structural basis for pregnenolone biosynthesis by the mitochondrial monooxygenase system. *Proc. Natl. Acad. Sci. USA.* **108**: 10139–10143.
28. Williams, P. A., J. Cosme, V. Sridhar, E. F. Johnson, and D. E. McRee. 2000. Mammalian microsomal cytochrome P450 monooxygenase: structural adaptations for membrane binding and functional diversity. *Mol. Cell.* **5**: 121–131.
29. Axelson, M., I. Bjorkhem, E. Reihner, and K. Einarsson. 1991. The plasma level of 7 alpha-hydroxy-4-cholesten-3-one reflects the activity of hepatic cholesterol 7 alpha-hydroxylase in man. *FEBS Lett.* **284**: 216–218.
30. Nakayama, K., A. Puchkaev, and I. A. Pikuleva. 2001. Membrane binding and substrate access merge in cytochrome P450 7A1, a key enzyme in degradation of cholesterol. *J. Biol. Chem.* **276**: 31459–31465.
31. Mast, N., S. E. Graham, U. Andersson, I. Bjorkhem, C. Hill, J. Peterson, and I. A. Pikuleva. 2005. Cholesterol binding to cytochrome P450 7A1, a key enzyme in bile acid biosynthesis. *Biochemistry*. **44**: 3259–3271.
32. Goizet, C., A. Boukhris, A. Durr, C. Beetz, J. Truchetto, C. Tesson, M. Tsaousidou, S. Forlani, L. Guyant-Marechal, B. Fontaine, et al. 2009. CYP7B1 mutations in pure and complex forms of hereditary spastic paraplegia type 5. *Brain*. **132**: 1589–1600.
33. Ullrich, V., and R. Brugger. 1994. Prostacyclin and thromboxane synthase: new aspects of hemethiolate catalysis. *Angew. Chem. Int. Ed. Engl.* **33**: 1911–1919.
34. Li, Y. C., C. W. Chiang, H. C. Yeh, P. Y. Hsu, F. G. Whitby, L. H. Wang, and N. L. Chan. 2008. Structures of prostacyclin synthase and its complexes with substrate analog and inhibitor reveal a ligand-specific heme conformation change. *J. Biol. Chem.* **283**: 2917–2926.
35. Breuer, O., E. Sudjana-Sugiaman, G. Eggertsen, J. Y. Chiang, and I. Bjorkhem. 1993. Cholesterol 7 alpha-hydroxylase is up-regulated by the competitive inhibitor 7-oxocholesterol in rat liver. *Eur. J. Biochem.* **215**: 705–710.
36. Shinkyo, R., L. Xu, K. A. Tallman, Q. Cheng, N. A. Porter, and F. P. Guengerich. 2011. Conversion of 7-dehydrocholesterol to 7-ketocholesterol is catalyzed by human cytochrome P450 7A1 and occurs by direct oxidation without an epoxide intermediate. *J. Biol. Chem.* **286**: 33021–33028.
37. Björkhem, I., U. Diczfalussy, A. Lövgren-Sandblom, L. Starck, M. Jonsson, K. Tallman, H. Schirmer, L. Bomme Ousager, P. J. Crick, Y. Wang, et al. 2014. On the formation of 7-ketocholesterol from 7-dehydrocholesterol in patients with CTX and SLO. *J. Lipid Res.* **55**: 1165–1172.
38. Headlam, M. J., M. C. Wilce, and R. C. Tuckey. 2003. The F-G loop region of cytochrome P450_{sc} (CYP11A1) interacts with the phospholipid membrane. *Biochim. Biophys. Acta.* **1617**: 96–108.
39. Lomize, M. A., I. D. Pogozheva, H. Joo, H. I. Mosberg, and A. L. Lomize. 2012. OPM database and PPM web server: resources for positioning of proteins in membranes. *Nucleic Acids Res.* **40**: D370–D376.
40. Baylon, J. L., I. L. Lenov, S. G. Sligar, and E. Tajkhorshid. 2013. Characterizing the membrane-bound state of cytochrome P450

- 3A4: structure, depth of insertion, and orientation. *J. Am. Chem. Soc.* **135**: 8542–8551.
41. Berka, K., T. Hendrychova, P. Anzenbacher, and M. Otyepka. 2011. Membrane position of ibuprofen agrees with suggested access path entrance to cytochrome P450 2C9 active site. *J. Phys. Chem. A*. **115**: 11248–11255.
 42. Lange, Y., J. Dolde, and T. L. Steck. 1981. The rate of transmembrane movement of cholesterol in the human erythrocyte. *J. Biol. Chem.* **256**: 5321–5323.
 43. Bruckner, R. J., S. S. Mansy, A. Ricardo, L. Mahadevan, and J. W. Szostak. 2009. Flip-flop-induced relaxation of bending energy: implications for membrane remodeling. *Biophys. J.* **97**: 3113–3122.
 44. Ost, T. W., A. W. Munro, C. G. Mowat, P. R. Taylor, A. Pessegueiro, A. J. Fulco, A. K. Cho, M. A. Cheesman, M. D. Walkinshaw, and S. K. Chapman. 2001. Structural and spectroscopic analysis of the F393H mutant of flavocytochrome P450 BM3. *Biochemistry*. **40**: 13430–13438.
 45. Monk, B. C., T. M. Tomasiak, M. V. Keniya, F. U. Huschmann, J. D. Tyndall, J. D. O'Connell III, R. D. Cannon, J. G. McDonald, A. Rodriguez, J. S. Finer-Moore, et al. 2014. Architecture of a single membrane spanning cytochrome P450 suggests constraints that orient the catalytic domain relative to a bilayer. *Proc. Natl. Acad. Sci. USA*. **111**: 3865–3870.
 46. Grochulski, P., M. N. Fodje, J. Gorin, S. L. Labiuk, and R. Berg. 2011. Beamline 08ID-1, the prime beamline of the Canadian Macromolecular Crystallography Facility. *J. Synchrotron Radiat.* **18**: 681–684.
 47. Otwinowski, Z., and W. Minor. 1997. Processing of X-ray diffraction data collected in oscillation mode. *Methods Enzymol.* **276**: 307–326.
 48. Kabsch, W. 2010. XDS. *Acta Crystallogr. D Biol. Crystallogr.* **66**: 125–132.
 49. Murshudov, G. N., P. Skubak, A. A. Lebedev, N. S. Pannu, R. A. Steiner, R. A. Nicholls, M. D. Winn, F. Long, and A. A. Vagin. 2011. REFMAC5 for the refinement of macromolecular crystal structures. *Acta Crystallogr. D Biol. Crystallogr.* **67**: 355–367.
 50. Bricogne, G., E. Blanc, M. Brandl, C. Flensburg, P. Keller, W. Paciorek, P. Roversi, A. Sharff, O. S. Smart, C. Vonrhein, et al. 2011. BUSTER version 2.8.0. Cambridge, United Kingdom: Global Phasing Ltd.
 51. Smart, O. S., T. O. Womack, C. Flensburg, P. Keller, W. Paciorek, A. Sharff, C. Vonrhein, and G. Bricogne. 2012. Exploiting structure similarity in refinement: automated NCS and target-structure restraints in BUSTER. *Acta Crystallogr. D Biol. Crystallogr.* **68**: 368–380.
 52. Evans, P. R., and G. N. Murshudov. 2013. How good are my data and what is the resolution? *Acta Crystallogr. D Biol. Crystallogr.* **69**: 1204–1214.
 53. Adams, P. D., P. V. Afonine, G. Bunkoczi, V. B. Chen, I. W. Davis, N. Echols, J. J. Headd, L. W. Hung, G. J. Kapral, R. W. Grosse-Kunstleve, et al. 2010. PHENIX: a comprehensive Python-based system for macromolecular structure solution. *Acta Crystallogr. D Biol. Crystallogr.* **66**: 213–221.